AGU ADVANCING EARTH AND SPACE SCIENCES

JAMES | Journal of Advances in Modeling Earth Systems®

RESEARCH ARTICLE
10.1029/2023MS003985

Reduction in the Tropical High Cloud Fraction in Response to an Indirect Weakening of the Hadley Cell

S. R. Monisha Natchiar[1], Mark J. Webb[2], F. Hugo Lambert[1], Geoffrey K. Vallis[1], Cyril J. Morcrette[1,2], Christopher E. Holloway[3], Denis E. Sergeev[4], and Ian Boutle[2,4]

[1]Department of Mathematics and Statistics, University of Exeter, Exeter, UK, [2]Met Office, Exeter, UK, [3]Department of Meteorology, University of Reading, Reading, UK, [4]Department of Physics and Astronomy, University of Exeter, Exeter, UK

Abstract Tropical high cloud cover decreases with surface warming in most general circulation models. This reduction, according to the "stability-iris" hypothesis, is thermodynamically controlled and linked to a decrease in the radiatively-driven clear-sky convergence, when the peak anvil clouds rise because of the rising isotherms. The influence of the large-scale dynamical changes on the tropical high cloud fraction remains difficult to disentangle from the local thermodynamic influence, given that the mean meridional circulation remains inextricably tied to the local thermodynamic structure of the atmosphere. However, using idealized general circulation model simulations, we propose a novel method to segregate the dynamical impact from the thermodynamic impact on the tropical high cloud fraction. To this end, our investigation primarily focuses on the mechanisms underpinning changes in the high cloud cover in the deep tropics in response to extratropical surface warming, when the tropical sea surface temperatures remain invariant. Net convective detrainment of ice cloud condensates decreases at the peak detrainment region, without a rise in its altitude. We also find that the importance of depositional growth of ice cloud condensates in controlling the high cloud fraction response in the deep tropics varies with altitude.

Plain Language Summary The cloud feedback associated with changes in the tropical high cloud cover is one of the major uncertainties in calculating the current estimates of climate sensitivity, which is a measure of how much the Earth's average surface temperature would increase if we double the amount of atmospheric carbon dioxide. When the surface becomes warmer in the tropics, the tropical high cloud cover decreases. However, this raises an important question: how do circulation changes independent of the temperature changes within the tropics impact the tropical high cloud cover? Using idealized general circulation model simulations, we found that the tropical high cloud fraction decreases as a result of circulation changes induced by extratropical warming, even when the tropical sea surface temperatures are held constant. Both convective and cloud microphysical processes play significant roles in controlling the changes in tropical high cloud fraction, and their relative importance varies with altitude. Understanding the different factors responsible for the changes in high cloud cover is important, as the area covered by these tropical high clouds can affect how much the Earth warms under climate change.

Key Points:

- An indirect weakening of the Hadley circulation decreases the convectively-detrained ice cloud condensates in the deep tropics
- A concurrent reduction in the net vertical transport of water vapor limits the depositional growth of ice cloud condensates
- The relative influence of depositional growth to net convective detrainment on the tropical high cloud response is altitude-dependent

Supporting Information:

Supporting Information may be found in the online version of this article.

Correspondence to:

S. R. M. Natchiar,
m.subbiah-renganathan@exeter.ac.uk

Citation:

Natchiar, S. R. M., Webb, M. J., Lambert, F. H., Vallis, G. K., Morcrette, C. J., Holloway, C. E., et al. (2024). Reduction in the tropical high cloud fraction in response to an indirect weakening of the Hadley cell. *Journal of Advances in Modeling Earth Systems*, *16*, e2023MS003985. https://doi.org/10.1029/2023MS003985

Received 22 AUG 2023
Accepted 25 APR 2024

Author Contributions:

Conceptualization: S. R. Monisha Natchiar, Mark J. Webb, F. Hugo Lambert, Geoffrey K. Vallis, Cyril J. Morcrette
Data curation: S. R. Monisha Natchiar
Formal analysis: S. R. Monisha Natchiar
Funding acquisition: F. Hugo Lambert, Geoffrey K. Vallis
Investigation: S. R. Monisha Natchiar

1. Introduction

Understanding the mechanisms that control the fractional coverage of tropical anvil clouds is crucial for improving estimates of Earth's climate sensitivity (Sherwood et al., 2020). The net cloud radiative effect of tropical anvil clouds formed from detrained cloud condensates of deep convective cores is approximately zero because of their counterbalancing shortwave (cloud albedo effect) and longwave effects (cloud greenhouse effect) (Hartmann & Berry, 2017). Nonetheless, the shortwave and longwave cloud radiative effects of these clouds are individually large (Harrison et al., 1990; Ramanathan et al., 1989); changes in the optical properties of these clouds can therefore have a significant impact on their radiative feedback with warming (Hartmann, 2016; Sherwood et al., 2020).

Tropical high cloud cover is projected to decrease with surface warming in the tropics (i.e., local warming), following the same fundamental thermodynamic principle that governs the peak height of the tropical anvil clouds, known as the Fixed Anvil Temperature or FAT hypothesis (Hartmann & Larson, 2002; Kuang & Hartmann, 2007). As surface warming causes isotherms to rise, the altitude at which maximum convective detrainment or the peak of anvil cloud fraction occurs is also predicted to increase (Zelinka & Hartmann, 2010,

Methodology: S. R. Monisha Natchiar, Mark J. Webb, F. Hugo Lambert
Software: S. R. Monisha Natchiar, Denis E. Sergeev
Supervision: Mark J. Webb, F. Hugo Lambert, Geoffrey K. Vallis, Christopher E. Holloway
Validation: S. R. Monisha Natchiar
Visualization: S. R. Monisha Natchiar
Writing – original draft: S. R. Monisha Natchiar
Writing – review & editing: S. R. Monisha Natchiar, Mark J. Webb, F. Hugo Lambert, Geoffrey K. Vallis, Cyril J. Morcrette, Christopher E. Holloway, Denis E. Sergeev, Ian Boutle

2011). This upward shift of high clouds to a more stable region of the atmosphere is expected to result in a reduction of the high cloud fraction, as per the stability-iris hypothesis (Bony et al., 2016; Zelinka & Hartmann, 2011). This mechanism arising out of thermodynamic constraints in the clear-sky region links the deep tropical high cloud changes to the changes in the radiatively-driven clear-sky convergence or upper-tropospheric dry static stability.

It is widely acknowledged that local surface warming (e.g., within the tropics), such as that caused by an increase in the concentration of greenhouse gases, is associated with an increase in the dry static stability (Knutson & Manabe, 1995). Evaluating this within the framework of the dry static energy budget (see Equation B1) would indicate that the subsidence velocity tends to decrease, as the dry static stability increases without a commensurate increase in the rate of radiative cooling within the subsidence regions (with the assumption that the change in the evaporative cooling rate remains negligible). Additionally, the absence of unreasonably large increases in latent heating in the tropical ascent regions, along with the decrease in subsidence velocity, implies a weakening of the tropical mean circulation with local surface warming (refer to Equation 9 of Jenney et al. (2020)). This in turn implies a reduction in the tropical convective mass flux (Jeevanjee, 2022). However, there is very limited insight into how changes in the circulation without the attendant temperature changes influence the high cloud changes in the deep tropics, given that the large-scale mean meridional (or Hadley) circulation is thermally direct and remains inextricably tied to the thermodynamic structure of the atmosphere.

To isolate the large-scale circulation (i.e., Hadley cell) changes from the thermodynamic changes in the tropics, we choose to warm the extratropics, keeping the tropical sea surface temperatures (SSTs) unchanged, and analyze their impact on the tropical high cloud fraction. The importance of extratropical eddy momentum and/or eddy energy fluxes in determining the strength of the Hadley cell has been explored in a number of studies, including Bordoni and Schneider (2008), Singh and Kuang (2016), Singh et al. (2017), and Kim et al. (2022) and the references therein. Nonetheless, the impact of eddy-induced changes in the mean circulation on the tropical high cloud fraction remains less explored. This is especially relevant because future changes in temperature and circulation may not replicate historical patterns or trends. Consequently, a comprehensive understanding of the interaction between circulation and small-scale processes, and how this impacts the tropical high clouds, is crucial for accurate predictions of climate change. This study will focus on the changes in the tropical high cloud fraction caused by changes in the mean meridional circulation owing to extratropical surface warming, while the tropical SSTs remain unchanged.

Some of the questions we aim to address in this study are: does the peak of tropical anvil clouds shift to higher altitudes and/or find themselves in a more stable environment in response to changes in the atmospheric dynamics induced by extratropical surface warming? In the absence of a significant free-tropospheric temperature increase in the tropics in response to extratropical warming, what governs the changes in the peak anvil cloud fraction? Given the decrease in the meridional temperature gradient, we expect a weakening of the Hadley circulation by the large-scale extratropical eddies. Does a weakened Hadley cell then cause a reduction in the tropical high cloud fraction by modulating the tropical convective mass flux?

Moreover, while the stability-iris hypothesis (Bony et al., 2016) suggests that the changes in the upper-tropospheric dry static stability play a primary role in determining changes in the high cloud fraction, the impact of cloud microphysical processes (among other factors) on the extent of high clouds in climate change scenarios remains less explored. Even with the stability-iris hypothesis finding some observational support (Saint-Lu et al., 2020), there are some modeling studies (Chen et al., 2016; Ohno & Satoh, 2018; Ohno et al., 2019; Singh & O'Gorman, 2015; Tsushima et al., 2014), and approximately one-third of the cloud-resolving models within the RCEMIP framework (Stauffer & Wing, 2022; Wing et al., 2020) that predict an expansion in the anvil cloud area with warming. Consequently, the relative importance of cloud microphysical processes in influencing the tropical high cloud coverage remains unclear.

More recently, Seeley et al. (2019) and Beydoun et al. (2021) have included sinks of ice cloud condensates as important terms in predicting cloud lifetime and therefore the anvil cloud fraction. Sinks of cloud condensates via precipitation, evaporation or sublimation and dilution or entrainment-mixing were found to be important in the accurate determination of the anvil cloud fraction. Seeley et al. (2019) defined anvil cloud fraction as the product of gross detrainment and a positive-definite cloud lifetime, emphasizing the significance of cloud microphysical timescales in determining the anvil cloud fraction. Using their diagnostic framework, Beydoun et al. (2021) further corroborated that both detrainment and cloud lifetime are crucial for accurately predicting anvil cloud

coverage. The role of cloud microphysical processes in determining anvil cloud fraction was also demonstrated in cloud-resolving simulations run in radiative-convective equilibrium using both a simple and a complex microphysics scheme (Jeevanjee, 2022). The study found that identical clear-sky convergence peaks did not yield similar anvil cloud fractions, attributing this discrepancy to variations in the microphysics schemes.

While incorporating a parameter that quantifies cloud decay is important for the accurate determination of anvil cloud lifetimes and therefore anvil cloud fraction as suggested in these studies, microphysical *sources* of ice cloud condensates, such as the depositional growth of ice cloud condensates, are also important as indicated in some other studies (Gasparini et al., 2019, 2022; Hartmann et al., 2018; Ohno et al., 2021). Understanding the influence of microphysical sources of ice cloud condensates on the tropical high cloud fraction using a general circulation model (GCM) is one focus of our study. Cloud ice mixing ratio that affects the anvil cloud lifetime has been found to be largely influenced by the net convective detrainment but also by the depositional growth of ice cloud condensates (Gasparini et al., 2021). Understanding the interplay between convective, advective and cloud microphysical processes in controlling the tropical anvil cloud fraction in GCMs is vital to constrain the "tropical anvil cloud area feedback," which is a major source of uncertainty in the estimation of equilibrium climate sensitivity.

This paper is organized as follows. Section 2 describes the model configuration used in this study, while Section 3 delves into the results, with the weakening of the Hadley circulation caused by extratropical surface warming explored in Section 3.1, and the two pathways leading to the reduction in the high cloud fraction investigated in Section 3.2. The paper ends with a discussion and conclusions presented in Section 4.

2. Model Configuration: Aquaplanet Simulations With Prescribed SSTs

Idealized aquaplanet simulations are performed using the Global Atmosphere 7.0 configuration of the Met Office Unified Model (Walters et al., 2019) in an atmosphere-only GCM setup with prescribed SSTs. The model employs a semi-implicit, semi-Lagrangian formulation to solve the three-dimensional non-hydrostatic, compressible equations of motion, and utilizes physical parameterizations to represent subgrid-scale processes such as atmospheric radiation, boundary-layer turbulence, convection, clouds, and precipitation. The model setup employs a single-moment microphysics scheme as described in Walters et al. (2019) that is primarily based on a modified Wilson and Ballard (1999) microphysics scheme. Here, only the mass mixing ratio of the hydrometeor species is determined prognostically, while the number concentration of the respective hydrometeor species is diagnosed. The model contains only one prognostic ice species (hereafter termed "aggregates"), but all microphysical process rates between the ice species (aggregates) and other water species are calculated using the generic ice particle size distribution of Field et al. (2007), ensuring that they can represent the whole range of ice particle size, from pristine crystals to large snow. Furthermore, a mass-flux convective parameterization scheme (Gregory & Rowntree, 1990) with adaptive detrainment (Derbyshire et al., 2011) and a CAPE-based closure is employed. Clouds are parameterized using either a prognostic (PC2 cloud scheme; Wilson et al. (2008)) or a diagnostic scheme (the Smith cloud scheme; Smith (1990)).

The model equations are integrated over a period of 20 years, with a horizontal resolution of 2.5° longitude by 2° latitude, and with 38 vertical levels between the surface and the model top at 40 km. The integration time step is fixed at 20 min. Monthly mean diagnostics are output at regular intervals. The last 15 years of simulation data are analyzed, discounting the initial 5 years to account for the spin-up period. More details on the model physics and parameterization schemes can be found in Boutle et al. (2017) and Walters et al. (2019).

Both the control (CTRL in Figure 1) and perturbed (PERT) simulations are forced with prescribed SSTs that spatially vary only along the meridional direction. The control SSTs are obtained from the steady-state zonal-mean SSTs of a 20-year simulation with a slab-ocean that are smoothed meridionally using a Gaussian kernel. Here, the slab-ocean has a heat capacity of 1×10^7 J K^{-1} m^{-2}, corresponding to a slab ocean depth of approximately 2.5 m. The CO_2 concentration is fixed at 594.1 ppm by weight. In the case of perturbed simulations (PERT), SSTs remain identical to the CTRL within the latitudinal bounds of ±30°N. Beyond these bounds in the extratropics (extending from ±30° to ±90°N), the increase in SSTs is linear as prescribed by $\Delta T = m\Delta\theta$, with $\Delta\theta$ denoting the latitudinal difference from 30° (i.e., $\Delta\theta = |\theta| - 30°$) and m representing the slope of linear increase set at 0.1 K per degree. This leads to a warming of 6 K at each pole. The model excludes any seasonality or sea ice components.

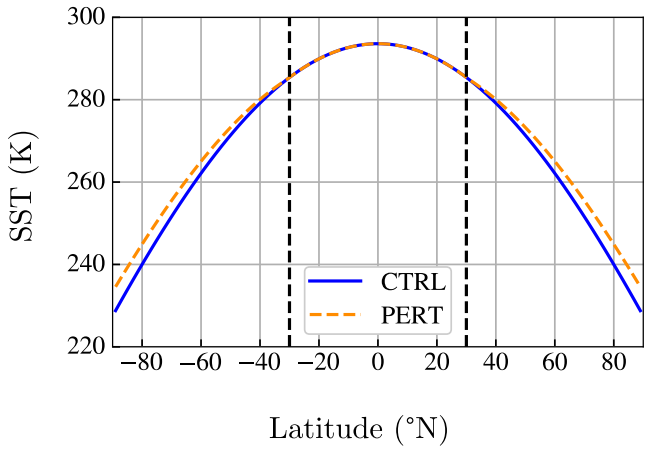

Figure 1. Prescribed zonal-mean sea surface temperatures (SSTs) in control (blue solid) and perturbed (orange dashed) aquaplanet simulations using the Unified Model. The SSTs remain unchanged in the tropics (between ±30°N latitudes).

3. Results

3.1. Weakening of the Hadley Circulation

The weakening of the Hadley circulation is depicted by the changes in the mass meridional stream function between the perturbed and control climates (i.e., $\psi_{PERT} - \psi_{CTRL}$), as shown in color in Figure 2. The corresponding stream function in the control climate is delineated using black curves. Regardless of whether a prognostic (panel a) or diagnostic cloud scheme (panel b) is used, the mean mass meridional circulation exhibits a comparable degree of weakening of at least 5% in the tropical mid-troposphere.

Our investigation is focused on the tropical ascent region, specifically between altitudes 8 and 12.5 km (i.e., the upper troposphere). We observe insignificant changes in the time-averaged fractional area of ascent within the tropics (determined using vertical velocity at 500 hPa). This result is apparently inconsistent with previous research by Schiro et al. (2019) and Jenney et al. (2020). However, it should be noted that Schiro et al. (2019) and Jenney et al. (2020) reported changes in the fractional area of ascent and/or high cloud fraction in response to *local* warming and not due to remote or extratropical warming as in the present study. This study predominantly aims to decipher the cause for the reduction in high cloud fraction that is observed in the tropical ascent region or the deep tropics, in light of the observed weakening of the Hadley circulation due to extratropical warming. Note that the terms "tropical ascent region" and "deep tropics" will be used interchangeably throughout the manuscript.

Our analysis reveals a decrease in the boundary layer specific humidity in the tropics as a result of extratropical warming (as shown in Figures 3e and 3f focusing on the tropics between latitudes ±30°N), which can be attributed to the lower branch of the Hadley circulation transporting reduced amounts of moisture into the deep tropics due to the weakened mean circulation (refer to Figures S1–S4 in Supporting Information S1 for moisture convergence by the mean flow and transient eddies; the Reynolds decomposition of the moisture convergence is given in Appendix A). This reduced influx of moisture subsequently leads to a decrease in the relative humidity (RH) within the region (Figures 3c and 3d), notwithstanding a slight reduction in the free-tropospheric temperature (Figures 3g and 3h).

The decrease in the free-tropospheric tropical temperature can be understood as a direct consequence of the tropical temperature profile adhering to a moist adiabat, thus conforming to a cooler moist adiabat in response to a reduced boundary layer equivalent potential temperature. The reduction in high cloud fraction (Figures 3a and 3b) aligns with a decrease in the RH (Figures 3c and 3d), and as will be shown in Figure 5, a decrease in the mass fraction of ice cloud condensates within the region. In the next section, we investigate the underlying mechanisms behind this relationship.

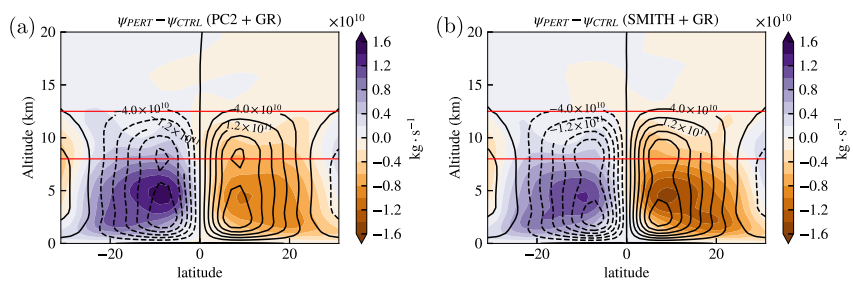

Figure 2. The imposed extratropical surface warming (not shown here) causes a weakening of the large-scale Hadley circulation, depicted here via a difference in the mass meridional stream function (ψ) between the perturbed and control climates (in color). Note that the latitude range shown is between ±30°N. The black contours represent ψ_{CTRL} with a contour spacing of 4×10^{10} kg · s^{-1}. Simulations are run with either a prognostic (PC2; panel (a)) or a diagnostic (Smith; panel (b)) cloud scheme, and a mass-flux convection scheme. A maximum Hadley cell weakening at 500 hPa is approximately 7% in simulations with the PC2 cloud scheme (panel a), and approximately 5% using the Smith scheme (panel b). The region of interest is demarcated by horizontal red lines at 8 and 12.5 km.

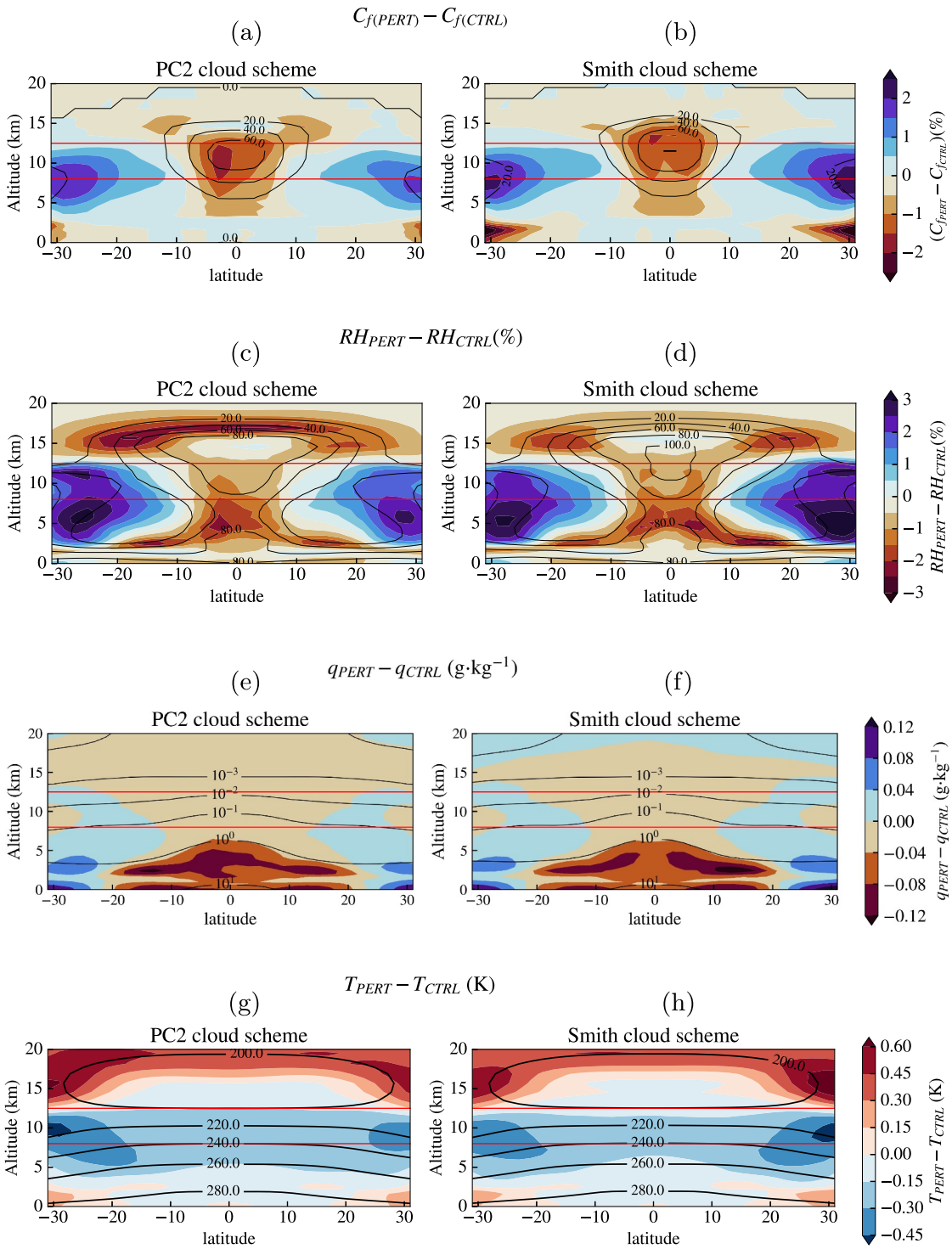

Figure 3. Contour plots showing responses of ice cloud fraction (C_f), relative humidity (RH), specific humidity (q), and air temperature (T) in the tropics (i.e., between ±30°N) to imposed extratropical surface warming (as shown in Figure 1). Control climate is represented using black contours and the response is shown in color. Panels (a and b) depict at least a 1% reduction in C_f in the tropical ascent region, which corresponds to a decrease in RH (c and d) and q (e and f) in the same region (between ±7° N), albeit a slight cooling of the mid- to upper troposphere (g and h). Simulations are run with a mass-flux (Gregory-Rowntree) convection scheme, and with either a prognostic (PC2; left panels) or diagnostic (Smith; right panels) cloud scheme.

3.2. Mechanisms Underpinning the Reduction in High Cloud Fraction

We examine the causes for the decrease in high cloud fraction within the deep tropics, employing two distinct physical pathways as outlined in Figure 4. Pathway I (in purple) illustrates the decrease in ice cloud fraction due to the reduced detrainment of ice cloud condensates resulting from a weakened Hadley circulation, while Pathway II (in green) details the reduction of ice cloud fraction caused by a decrease in the depositional growth of ice cloud condensates. Both pathways lead to a decrease in the mass fraction of ice cloud condensates in the upper troposphere of the tropical ascent region, which strongly correlates with a decline in the high cloud fraction. Refer to Figure 5 which shows a high correlation in terms of both Pearson (r) and distance correlation (r_D) coefficients between changes in the mass fraction of ice cloud condensates (Δq_{cf}) and ice cloud fraction (ΔC_f) in the deep tropical upper troposphere; note that the distance correlation coefficient (Chaudhuri & Hu, 2019; Székely et al., 2007) is a non-linear correlation metric between any two random variables, without strict assumptions about their distributions. It is more robust than Pearson correlation, which assumes normality and can only quantify linear relationships. Some important properties of the distance correlation coefficient (r_D) between any two random variables X and Y are: (a) $0 \leq r_D(X,Y) \leq 1$, (b) $r_D(X,Y) = 0$ iff X and Y are independent.

Evaluating both pathways requires a prognostic (PC2) cloud scheme, which enables a prognostic detrainment of ice cloud condensates, allowing them to respond more accurately to environmental changes through the large-scale microphysics scheme. This study also incorporates a diagnostic cloud scheme to assess the parameterization dependence of the cloud fraction response (see Figure S8 in Supporting Information S1). Figures 5–10 utilize only the prognostic cloud scheme. Although the Smith scheme diagnoses q_{cf} based on the detrained water vapor from the convection scheme, its cloud fraction response is comparable to that of the PC2 scheme (see Figure S8 in Supporting Information S1). An explicit mathematical formulation relates C_f to q_{cf} in the Smith scheme, (see Equation A1 in Abel et al. (2017)), while it appears as an emergent property in the PC2 scheme as shown in Figure 5.

In the following subsections, we describe Pathway I (Section 3.2.1) and Pathway II (Section 3.2.2) in more detail. More details on the microphysical transfer terms for the tendency of ice cloud condensate mixing ratio (denoted as m_{cf}) can be found in Figure S5 of Supporting Information S1. The depositional growth of ice condensates is the dominant microphysical *source* of ice cloud condensates in the deep tropical upper troposphere. It is noteworthy that the sublimation rate of ice is negligible above 5 km. Note that the cloud ice mixing ratio (m_{cf}; kg per kg of dry air) is approximately equal to the mass fraction of ice cloud condensates (q_{cf}; kg per kg of moist air) in the region of interest.

3.2.1. Pathway I or Convective Pathway: Decrease in the Net Detrainment of Ice Cloud Condensates

Pathway I for the decrease in high cloud fraction is investigated through Figures 6–8. Both physical pathways are premised on the understanding that extratropical warming causes a weakening of the mean meridional circulation (see Figure 2; Figures S1 and S2 in Supporting Information S1). Based on the principles of mass conservation, and given the negligible changes in the subsidence (or ascent) area fraction within the tropics, it follows that there is a corresponding reduction in the convective mass flux within the region of tropical large-scale ascent (see Figures 6a and 6b). It is worth mentioning that although the studies conducted by Jenney et al. (2020) and Jeevanjee (2022) have yielded similar results, specifically a decrease in convective mass flux in the tropical ascent region with warming, their research focused on local surface warming, which presents a different context from our current study.

Within the region characterized by peak net detrainment and hence peak anvil cloud fraction (specifically, around an altitude of 11.5 km), we observe a reduction in the net convective detrainment of mass flux (as shown in Figures 6c and 6d). Assuming no significant changes in the precipitation efficiency within the convection scheme (a simple microphysics scheme is included within the mass-flux convection scheme that immediately rains out excess condensates above a certain threshold depending on the environmental saturation specific humidity), we expect a corresponding decrease in the net detrainment of ice cloud condensates into the upper troposphere. Note that the reduction in the mass fraction of ice cloud condensates exhibits a strong correlation with that of ice cloud fraction (Figure 5). Consequently, the factors influencing changes in the mass fraction of ice cloud condensates would have a significant impact on the changes in ice cloud fraction in the deep tropical upper troposphere.

A minor increase in the net detrainment of mass flux is observed between altitudes 8 and 9 km, a transitional region between net entrainment in the mid-troposphere and net detrainment in the upper troposphere (Figures 6c and 6d). While changes in the net convective detrainment significantly impact the reduction of ice cloud fraction near the peak net detrainment region, phase change and precipitation processes become crucial between 8 and

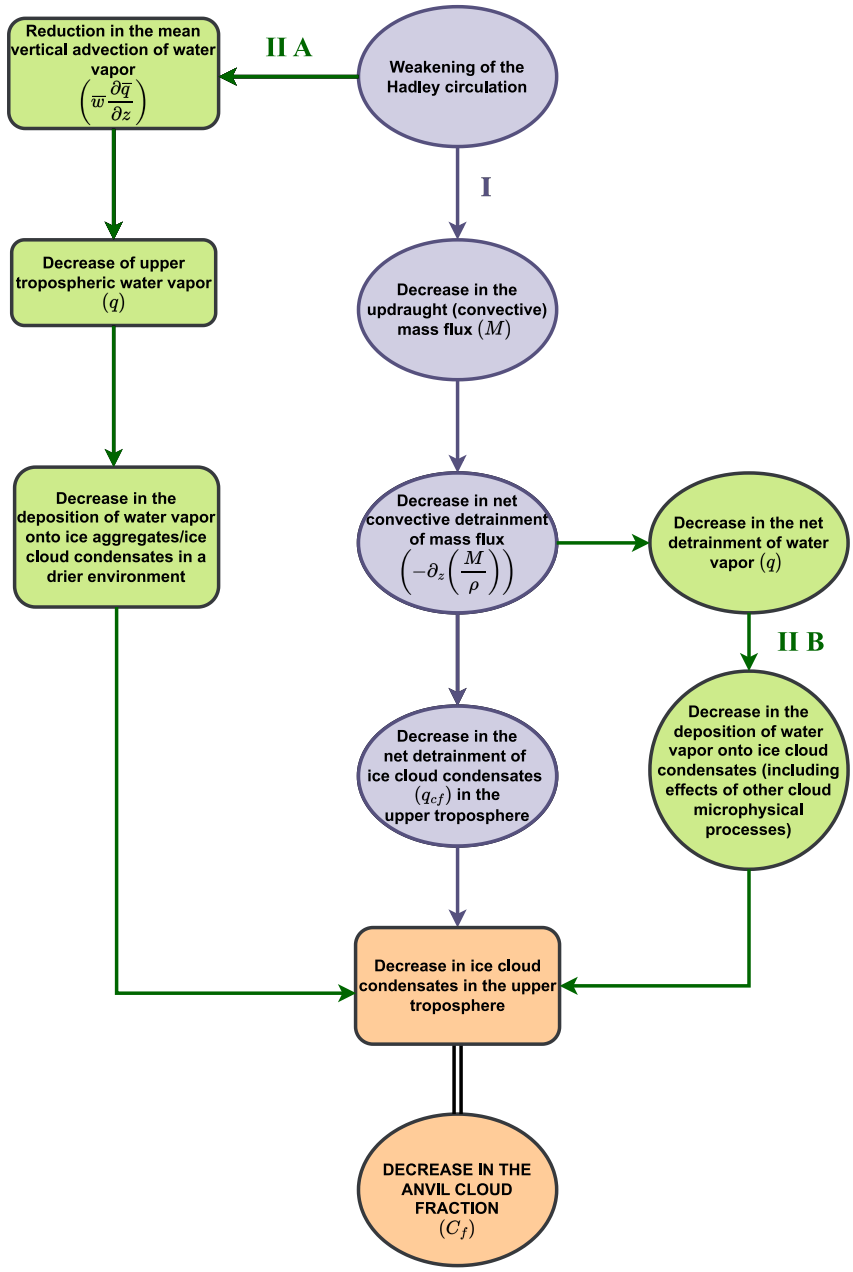

Figure 4. Schematic illustrating the causal links between high cloud reduction in the deep tropics and various environmental and cloud microphysical factors. Pathway I (purple) primarily represents the decrease in high clouds caused by reduced convective detrainment of mass flux due to a weakened Hadley circulation. Pathway II (green) highlights the dominant role of cloud microphysics, specifically the deposition of water vapor onto ice aggregates, which in turn is linked to the mean vertical advection of water vapor ($\bar{w}\partial\bar{q}/\partial z$) (II A) and a reduced convective detrainment of water vapor (II B). For further details on the derivation of moisture convergence, refer to Appendix A.

10 km. This is supported by Figures 6c–6f and 7, and further by Figures S11 and S12 in Supporting Information S1 that show the joint probability density function between changes in the ice cloud fraction and net convective detrainment or convective tendency of q_{cf}, respectively.

For instance, Figure 7a shows a strong correlation between changes in net detrainment of mass flux and ice cloud fraction near the peak net detrainment region (around 11.5 km), while the correlation is weak at the lower altitudes between 8 and 10 km. While the convective tendency of q_{cf} is predominantly influenced by the convective entrainment and detrainment processes, it also takes into account the phase change and precipitation processes that are modeled within the convection scheme. This presumably increases the correlation coefficient between the

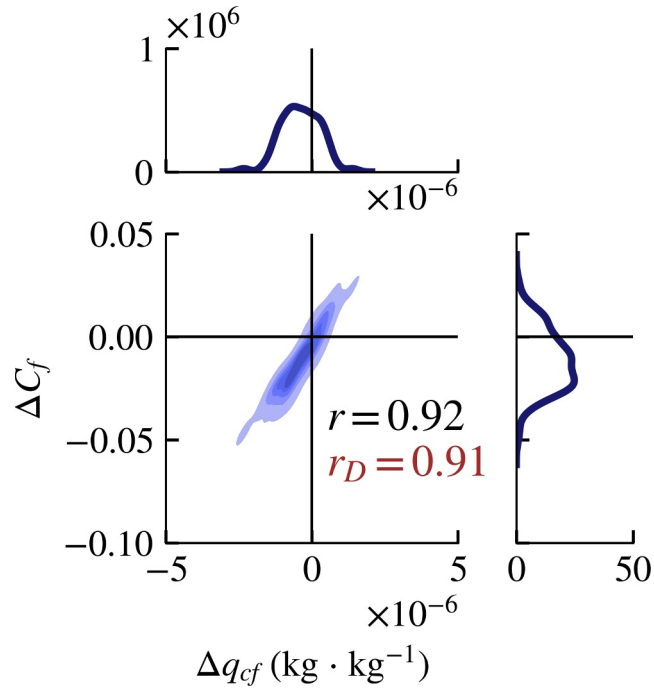

Figure 5. Kernel density estimates (KDE) for the joint probability density function of the zonal and annual-mean mean changes in ice cloud fraction (ΔC_f) and the mass fraction of ice cloud condensates (Δq_{cf}) are depicted within the altitude range of 8–12.5 km. The corresponding Pearson ($r = 0.92$) and distance correlation coefficients ($r_D = 0.91$) reveal a strong positive correlation between ΔC_f and Δq_{cf}. Each data point represents the zonal and annual-mean quantities for a specific latitude and vertical level in the tropical ascent region, with a total of 720 points (15 years × 8 latitudinal points × 6 vertical levels) used to construct the KDE plot.

changes in the ice cloud fraction and convective tendency of q_{cf} in the lower altitude range (Figure 7b; also see Figure S12 in Supporting Information S1), compared to that due to net detrainment alone (Figure 7a). The respective coefficients of linear regression are shown in Figures 7d and 7e. For the "bulk" updraft cloud model within the Gregory-Rowntree convection scheme that includes phase change and precipitation processes, see Appendix C (specifically Equation C3 for the sum of liquid and ice condensate fluxes).

3.2.2. Pathway II or Large-Scale Microphysical Pathway: Importance of Phase-Change and Precipitation Processes: Decrease in the Deposition of Water Vapor Onto Ice Cloud Condensates

The importance of cloud microphysical processes as a *source* of ice cloud condensates, such as deposition of water vapor onto ice cloud condensates, in determining the ice cloud fraction response to extratropical warming is explored in Pathway II.

While a leading-order influence of convective processes on q_{cf} is apparent above an altitude of 10 km, as shown in Figure 8a depicting the ratio of changes in convective to depositional tendencies of q_{cf}, the critical contribution of depositional growth of ice cloud condensates between the altitude range of 8–10 km is highlighted in Figure 8b that shows its corresponding inverse ratio. Between 8 and 10 km, the changes in the tendency of ice cloud condensates ($\Delta(\partial q_{cf}/\partial t)$) resulting from deposition become comparable to those due to convection (see Figure 8b), and are strongly correlated to the changes in ice cloud fraction (Figure 7c). The increase in the magnitude of the regression coefficient with altitude (Figure 7f) is reflective of the fact that changes in the depositional tendency of q_{cf} decreases significantly with altitude; above 10 km, the changes in the depositional tendency of q_{cf} are at least an order of magnitude smaller than at the lower altitudes (8–10 km). This is further supported by Figures S12 and S13 in Supporting Information S1. Here, for comparative clarity, changes in the depositional tendency $\left(\Delta\left(\partial q_{cf}/\partial t\right)_{dep}\right)$ are plotted on the same horizontal scale as the convective tendency of q_{cf} $\left(\Delta\left(\partial q_{cf}/\partial t\right)_{conv}\right)$, against ice cloud fraction changes along the vertical axis.

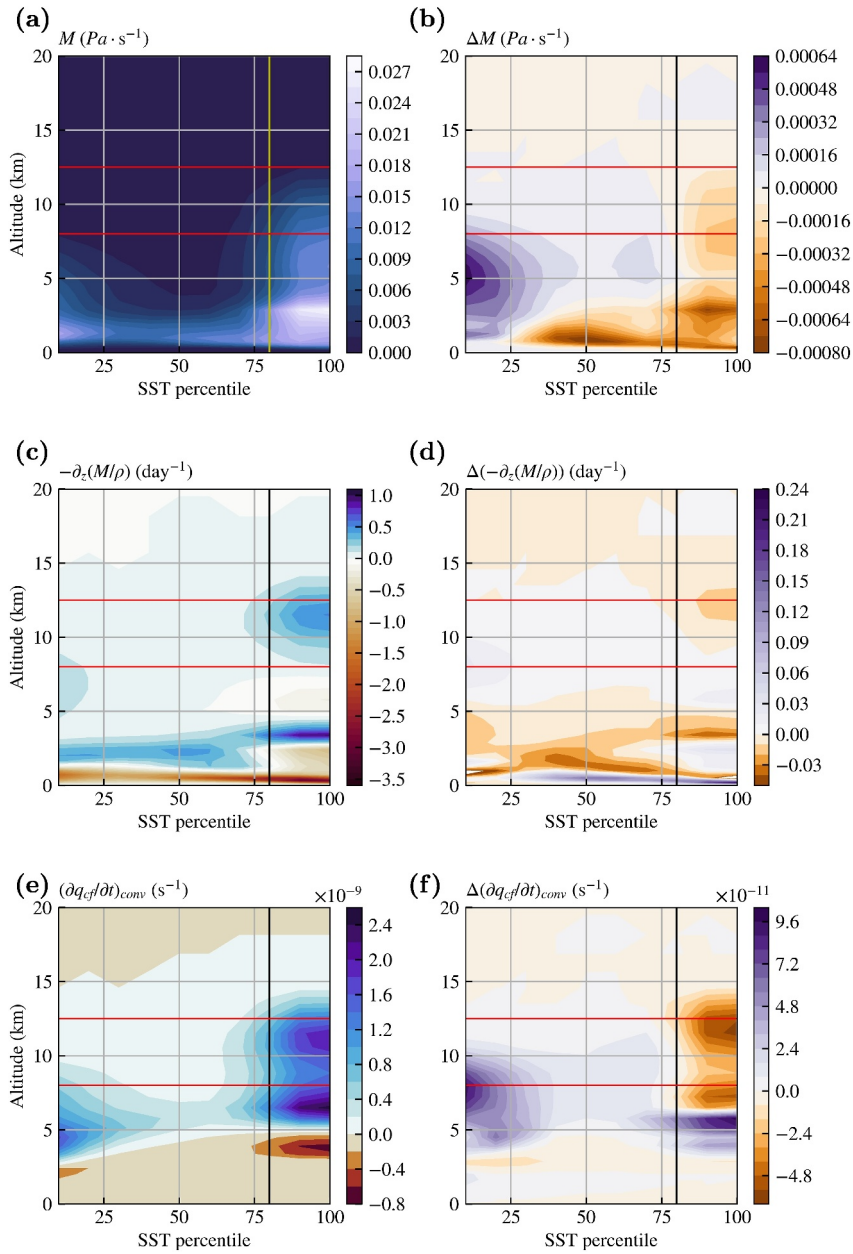

Figure 6. Binned monthly-mean data as a function of local (i.e., tropical) sea surface temperature (SST) percentiles for updraft mass flux (M), net convective detrainment of mass flux ($-\partial_z(M/\rho)$), and tendency of ice cloud condensates due to convection ($(\partial q_{cf}/\partial t)_{conv}$) in the control climate (panels (a, c, e)); their corresponding response values are plotted in the right panel (panels (b, d, f)). The 80th SST percentile (black vertical line) in both the control (left panels) and the response (right panels) separates the large-scale tropical ascent from the tropical descent region. The vertical profile of the convective mass flux averaged over the tropical ascent region is shown in Figure S7 of Supporting Information S1, with those of q_{cf} and ice cloud fraction shown in Figures S6 and S8 of Supporting Information S1, respectively.

Upon further investigation, it becomes evident that the primary reason for the decrease in the large-scale microphysical tendency of q_{cf} attributed to deposition is a reduction in the advective tendency of water vapor. Within the altitude range of 8–10 km, the decrease in water vapor advective tendency is at least two orders of magnitude larger than at the peak net detrainment region (illustrated in Figure S14 of Supporting Information S1). This leads to decreased mean environmental water vapor within the tropical ascent region, subsequently limiting the growth of ice cloud condensates via water vapor deposition onto pre-existing particles. That is, a drier

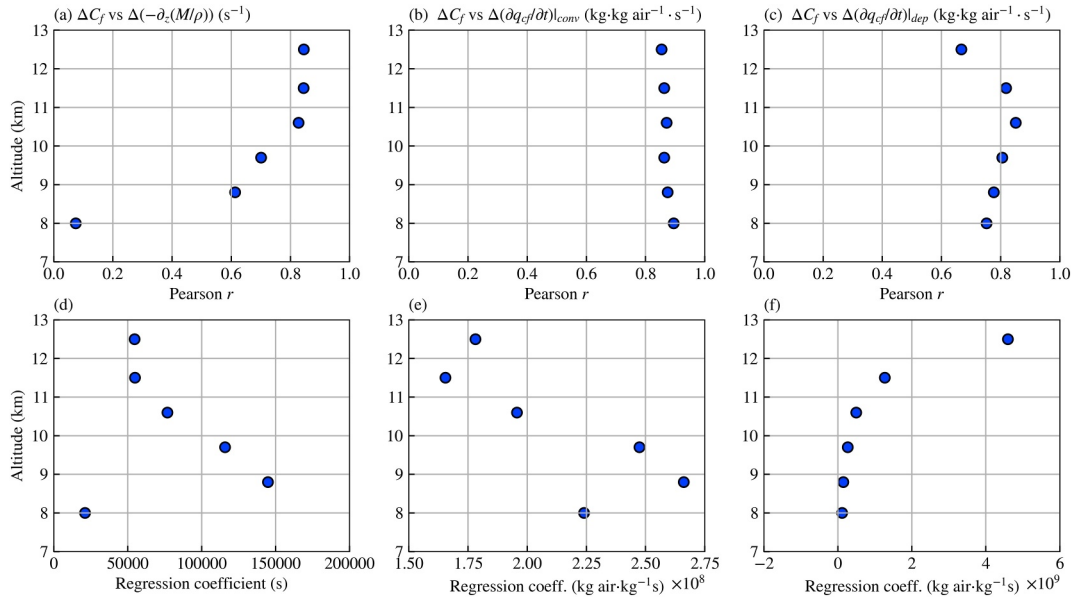

Figure 7. Pearson correlation and regression coefficients between changes in ice cloud fraction and net convective detrainment (panels a and d), convective tendency of q_{cf} (panels b and e), and depositional tendency of q_{cf} (panels c and f) at different altitudes between 8 and 12.5 km. As in Figure 5, zonal, annualmean quantities at each latitude in the tropical ascent region over 15 simulation years are considered to find the correlation and linear regression coefficients. The respective Kernel density estimates plots can be found in the supplementary.

environment decreases the depositional growth of ice condensates. The reduction in the mean vertical advection of water vapor in the upper troposphere of tropical ascent region, evident in Figure 9, further corroborates the decrease in the advective tendency of water vapor within the altitude range considered. For a complete description and/or visualization of the tendency terms in the water vapor and q_{cf} budget, please refer to Figures S9 and S10 in Supporting Information S1, respectively.

Cloud microphysical processes play a pivotal role not only as a sink term (Beydoun et al., 2021; Seeley et al., 2019), but as has been demonstrated, also as a *source* term for q_{cf} within the large-scale ascent region of the

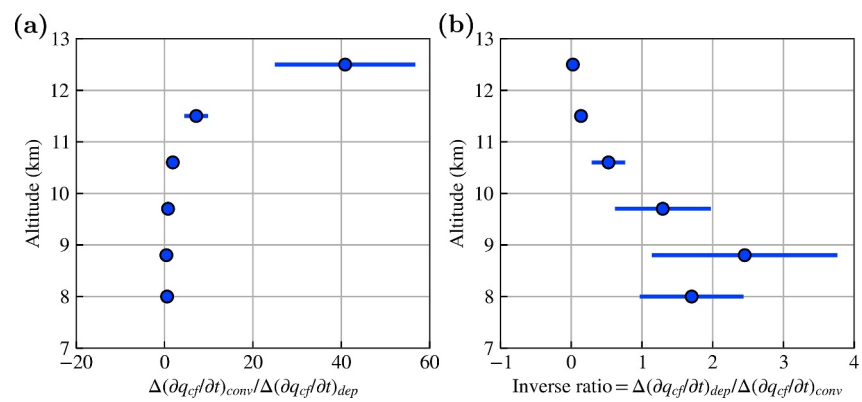

Figure 8. (panel a) Ratio and (panel b) inverse ratio of the changes in convective tendency of mass fraction of cloud ice $\left(\Delta\left(\frac{\partial q_{cf}}{\partial t}\right)_{conv}\right)$ to its depositional tendency $\left(\Delta\left(\frac{\partial q_{cf}}{\partial t}\right)_{dep}\right)$ are plotted. Panel (a) shows the leading-order influence of net convective detrainment in controlling ice cloud condensates and therefore ice cloud fraction near the peak net detrainment region (above 10 km). Panel (b) clearly depicts the importance of depositional growth of ice cloud condensates over its convective tendency between the altitude range of 8–10 km. The monthly- and zonal-mean quantities averaged over the tropical ascent region over a period of 15 simulation years are represented by filled circles, with error bars indicating 95% confidence intervals. A total of 1,440 data points (180 months × 8 latitudinal points in the tropical ascent region) are used to construct the error bars.

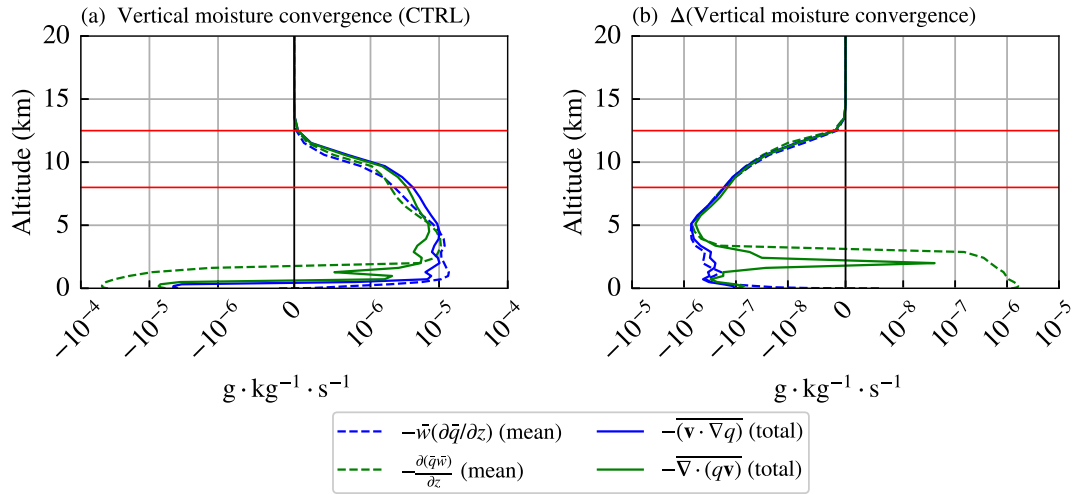

Figure 9. Vertical profiles of the vertical moisture convergence by the mean flow (green dashed) and the total moisture convergence (green solid) for the control simulation and their response to extratropical warming are shown in subfigures (a) and (b) respectively. The vertical and total advective terms of moisture are also plotted as blue dashed, and blue solid curves, respectively. The weakening of the mean vertical advection (blue dashed) dominates the reduction in the total moisture convergence (green solid), leading to a reduced moistening of the upper troposphere in the perturbed simulation. The detailed derivation of the decomposition of the total moisture flux convergence $\left(-\overline{\nabla\cdot(q\mathbf{v})}\right)$ into contributions from the mean flow and transient eddies, which are again expressed as a sum of advective $\left(-\overline{\mathbf{v}\cdot\nabla q}\right)$ and flow convergence $\left(-\overline{q(\nabla\cdot\mathbf{v})}\right)$ terms, is given in Appendix A. Additional figures that illustrate the different decomposed terms are plotted in the supplementary (see Figures S2–S4 in Supporting Information S1).

tropical upper troposphere. The importance of cloud microphysical processes as a source term, primarily through deposition of water vapor onto ice condensates, is particularly noticeable between 8 and 10 km as can be seen in Figure 8b. It is evident that there is a decrease in the depositional tendency of ice cloud condensates in the region of interest from Figure 10a showing the depositional tendency of q_{cf} in the control climate, and Figure 10b that depict their response to a weakened Hadley circulation caused by extratropical warming.

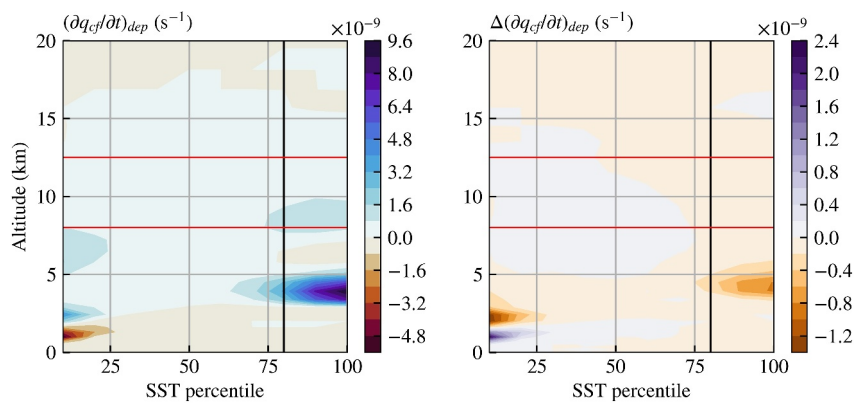

Figure 10. Binned monthly-mean data of the tendency of mass fraction of ice cloud condensates due to deposition of water vapor $\left(\left(\partial q_{cf}/\partial t\right)_{dep}\right)$ as a function of local sea surface temperature (SST) percentiles is presented. The 80th SST percentile separating the large-scale tropical ascent and descent regions is represented by a black vertical line in both the control (left panel) and the response (right panel). The analysis includes data from all longitudes within the tropics (±30°N) and reveals a reduction in the deposition throughout the tropical free troposphere in the large-scale ascent region.

4. Discussion and Conclusions

Through idealized aquaplanet simulations, we have investigated the factors influencing the reduction in the fractional coverage of tropical high clouds in the large-scale ascent region, in response to an indirectly weakened Hadley circulation caused by extratropical surface warming.

Our study specifically examined the relative importance of the impact of net convective detrainment and cloud microphysical processes, with a focus on the depositional growth of ice cloud condensates. We have identified two key physical pathways driving changes in the tropical high cloud coverage via changes in the mass fraction of ice cloud condensates: the first pathway involves net convective detrainment acting as the primary source of ice cloud condensates, particularly near the peak net detrainment region at around 11.5 km in the upper troposphere (pathway I), while the influence of grid-scale microphysical processes, *viz.* the deposition of water vapor onto ice cloud condensates is explored via the second pathway (pathways IIA and IIB). The influence of the depositional growth of ice cloud condensates is particularly significant within the altitude range of 8–10 km that forms the transition zone between mid-tropospheric net entrainment and upper-tropospheric net detrainment.

The stability-iris hypothesis suggests a decrease in the anvil cloud fraction with local warming, as the clouds ascend to a more stable atmosphere following the rising isotherms (Fixed Anvil Temperature or FAT hypothesis; Hartmann and Larson (2002)). When clouds ascend to lower pressure levels in these local warming scenarios, they encounter a more stable environment, resulting in a reduced detrainment of moisture and condensates. While we observe a slight increase in dry static stability near the tropopause associated with extratropical warming (refer to Figures S15 and S16 in Supporting Information S1), we do not observe a concomitant increase in the upper-tropospheric temperature, nor a rise in the altitude at which deep convecting clouds detrain water vapor and condensates. In contrast to local warming scenarios, our results show a slight cooling of the upper troposphere, attributed to the moist air parcels following a colder moist adiabat due to a reduced boundary layer equivalent potential temperature. It should be emphasized that while the stability-iris hypothesis explains the thermodynamic regulation of the tropical anvil cloud amount associated with local warming, it may not adequately address the dynamic influences on the anvil cloud fraction resulting from large-scale circulation changes that are independent of local SST changes. A significant reduction in the anvil cloud fraction in the deep tropics, as shown in Figures 3a and 3b and Figure S8 in Supporting Information S1, can occur even without a corresponding significant rise in the upper-tropospheric stability (see Figure S15 in Supporting Information S1; cf. Figure 7 of Bony et al. (2016)).

We ascribe the decrease in the mass fraction of ice cloud condensates, and thereby ice cloud fraction seen in our simulations (in the vicinity of the region of peak net detrainment) mainly to a decrease in the net detrainment of mass flux due to a reduced updraft mass flux. Assuming negligible changes in the precipitation efficiency accompanying the dynamical changes induced by extratropical warming, this would imply a reduced net detrainment of ice cloud condensates and water vapor in this region.

Related to previous works (e.g., Ohno and Satoh (2018) and Gasparini et al. (2021)), we have found that the depositional growth of ice cloud condensates plays a crucial role in controlling the tropical high cloud fraction, but we show that this is also the case when the tropical SSTs remain invariant. This is particularly relevant in the lower part of the tropical upper troposphere (between 8 and 10 km). Our results indicate that the relative importance of cloud microphysical processes over net convective detrainment is altitude-dependent. Although sedimentation of ice aggregates is found to dominate the microphysical tendency of q_{cf}, consistent with the study by Beydoun et al. (2021), we found that the microphysical *sources* of q_{cf} like the depositional growth of ice aggregates (refer to Figure 1 of Morrison et al. (2020)), also seem to be important. Heterogeneous and homogeneous ice nucleation processes have not been found to significantly affect the mass fraction of ice cloud condensates in our simulations, and secondary ice production processes were not considered.

The decrease in the depositional growth of ice aggregates with extratropical warming is a consequence of reduced environmental water vapor in the tropical ascent region. The resolved large-scale vertical motion carries less moisture into the tropical upper troposphere (i.e., reduced mean vertical advection), resulting in a decreased specific humidity and RH in the region. Note the slight cooling of the free-troposphere with extratropical warming. The decrease in the RH in the tropical upper troposphere is caused by a reduced moisture advected by

the weakened large-scale circulation. There is also a decrease in the convectively detrained water vapor into the upper troposphere of the tropical ascent region. In reality, however, moisture is almost exclusively carried upwards within narrow cloudy updrafts in the tropical free-troposphere due to positive static stability. The large-scale mean upward transport of water vapor in the deep tropics is then a balance between relatively large upward transport within narrow updrafts and downward transport within the broad environment exhibiting weak subsidence. General Circulation Models (GCMs), on the other hand, partition this moisture transport into transport done by the convection scheme, for which the upward mass flux must be exactly compensated by subsidence within an individual grid cell and convective time step, and a large-scale resolved flow governed by pressure gradients resulting from grid-mean increments including warming from this convective parameterization step. This implies that there can be *ascent* in GCM-resolved flow, which therefore transports water vapor upward on average, while water vapor in the real world (or in fine-grid explicit convection simulations) would be carried upward only in narrow convective updrafts. In our framework, pathway IIA (see Figure 4) describes the interaction between GCM-resolved large-scale flow and the parameterized grid-scale cloud microphysical processes (e.g., depositional growth of ice cloud condensates), whereas pathway IIB describes the interaction between the parameterized convection and parameterized grid-scale cloud microphysics.

The convective parameterization scheme and its impact on the large-scale environment may thus have implications on how the convective, advective and microphysical processes interact with one another in a GCM. Further investigations using either super-parameterization schemes or cloud-resolving simulations may therefore be necessary to test the robustness of these results. An important caveat to consider is that the strong correlation that emerges between Δq_{cf} and ΔC_f using the prognostic (PC2) cloud scheme might not accurately reflect real-world phenomena or the behavior seen in cloud-resolving models. The domain-averaged q_{cf} in these cases are typically controlled by q_{cf} within the convective cores, whereas cloud fraction is largely determined by the horizontal spreading or thinning of detrained anvil clouds. GCMs lack the capability to accurately simulate the subgrid-scale processes responsible for the spreading and thinning of the detrained anvil clouds. Consequently, when these processes are adequately resolved, it is possible that a decrease in domain-mean q_{cf} can be associated with an increase in ice cloud fraction and vice-versa, as evidenced in Figures 13a and 13b in Wing et al. (2020) and Figures 3a and 3c in Sokol and Hartmann (2022). This emphasizes the need for further investigation using cloud-resolving models to evaluate the GCM performance. In addition, substantial differences between single- and double-moment schemes principally attributed to sedimentation and rain evaporation rates have previously been reported, highlighting the advantages of using double-moment microphysics schemes (Field et al., 2023; Igel et al., 2015). However, the utility of double-moment schemes for the accurate representation of microphysical *sources* warrants further study.

Appendix A: Moisture Convergence by the Mean Flow and Transient Eddies

The atmospheric water vapor budget can be written as $\partial q/\partial t + \nabla \cdot (q\mathbf{v}) = E - P$, where E and P are the local evaporation and precipitation rates respectively. Considering steady-state, we have

$$-\nabla \cdot (q\mathbf{v}) = P - E. \tag{A1}$$

This equation represents the equivalence between the local moisture flux convergence and the local net precipitation. Decomposing the specific humidity (q) and wind vector ($\mathbf{v}$) into mean and transient eddy components, we have

$$-\nabla \cdot (q\mathbf{v}) = -\nabla \cdot \left(\left(\bar{q} + q'\right)\left(\bar{\mathbf{v}} + \mathbf{v}'\right)\right) = -\nabla \cdot \left(\bar{q}\bar{v} + \bar{q}\mathbf{v}' + q'\bar{\mathbf{v}} + q'\mathbf{v}'\right). \tag{A2}$$

Here, overbar denotes the time-mean and the prime notation represents transient eddy components which are deviations of the quantities from their respective time-means. Taking the time-mean of the total moisture convergence term, we arrive at the Reynolds decomposition

$$-\overline{\nabla \cdot (q\mathbf{v})} = -\nabla \cdot (\bar{q}\bar{\mathbf{v}}) - \overline{\nabla \cdot q'\mathbf{v}'}, \tag{A3}$$

since by definition, the time-means of $\bar{q}\mathbf{v}'$ and $q'\bar{\mathbf{v}}$ are zero. Using the product rule of divergence, this becomes

$$-\overline{\nabla\cdot(q\mathbf{v})} = \underbrace{-\bar{q}(\nabla\cdot\bar{\mathbf{v}}) - \bar{\mathbf{v}}\cdot\nabla\bar{q}}_{\text{mean component}} \underbrace{-\overline{q'\left(\nabla\cdot\mathbf{v}'\right)} - \overline{\mathbf{v}'\cdot\nabla q'}}_{\text{eddy component}}, \tag{A4}$$

Here, $-\bar{q}(\nabla\cdot\bar{\mathbf{v}})$ signifies the mean flow convergence weighted by the mean specific humidity, and $-\overline{q'\left(\nabla\cdot\mathbf{v}'\right)}$ signifies the eddy flow convergence weighted by its respective specific humidity, while $-\bar{\mathbf{v}}\cdot\nabla\bar{q}$ and $-\overline{\mathbf{v}'\cdot\nabla q'}$ denote the respective advection of moisture by the mean and eddy flows. The above equation can be further decomposed into horizontal and vertical components as

$$\begin{aligned}-\overline{\nabla\cdot(q\mathbf{v})} = \; & -\bar{q}(\nabla_h\cdot\bar{\mathbf{v}}_h) - \bar{q}\frac{\partial\bar{w}}{\partial z} - \overline{\mathbf{v}_h}\cdot\nabla_h\bar{q} - \bar{w}\frac{\partial\bar{q}}{\partial z} \\ & -\overline{q'\left(\nabla\cdot\mathbf{v}_h'\right)} - \overline{q'\frac{\partial w'}{\partial z}} - \overline{\mathbf{v}_h'\cdot\nabla_h q'} - \overline{w'\frac{\partial q'}{\partial z}},\end{aligned} \tag{A5}$$

where the wind vector $\mathbf{v} = (u, v, w)$ along the zonal (λ), meridional (ϕ) and vertical (z) directions. The subscript $_h$ denotes the corresponding horizontal component. The horizontal component of the divergence of a vector $\mathbf{A}$ is, for example, defined as

$$\nabla_h\cdot\mathbf{A}_h = \frac{1}{R\cos\phi}\left(\frac{\partial A_\lambda}{\partial\lambda} + \frac{\partial(A_\phi\cos\phi)}{\partial\phi}\right), \tag{A6}$$

where A_λ and A_ϕ are the zonal and meridional components of the vector $\mathbf{A}$ and R is the radius of the Earth.

Appendix B: Subsidence Vertical Velocity

The expression for the domain-mean subsidence velocity ($\bar{w}_{sub}$), derived from the dry static energy budget under the assumption of steady-state and weak temperature gradient within the tropics, is given by (Jeevanjee, 2022; Jenney et al., 2020):

$$\bar{w}_{sub} = \frac{\bar{\mathcal{H}}_{rad} + \bar{\mathcal{H}}_e}{\Gamma_d - \Gamma}, \tag{B1}$$

where $\bar{\mathcal{H}}_{rad} = \bar{Q}_{rad}/C_p$ and $\bar{\mathcal{H}}_e = \bar{Q}_e/C_p$ denote the diabatic heating terms in K/s, representing radiative and evaporative cooling rates (i.e., $\bar{\mathcal{H}}_{rad} < 0, \bar{\mathcal{H}}_e < 0$), respectively, and Γ_d and Γ represent the dry and moist adiabatic lapse rates.

Appendix C: Bulk Updraft Cloud Model

The equations for the bulk updraft cloud model, following Yanai et al. (1973), are given as below.

Mass flux, M^P:

$$-\frac{\partial\left(M^P\right)}{\partial p} = E - N - D, \tag{C1}$$

Moisture flux:

$$-\frac{\partial\left(M^P q^P\right)}{\partial p} = Eq^E - Nq^N - Dq^R - Q, \tag{C2}$$

Sum of liquid and frozen condensate fluxes:

$$-\frac{\partial\left(M^P q_{cl}^P + M^P q_{cf}^P\right)}{\partial p} = E\left(q_{cl}^E + q_{cf}^E\right) - N\left(q_{cl}^N + q_{cf}^N\right) - D\left(q_{cl}^R + q_{cf}^R\right) + Q - P. \tag{C3}$$

Here, the parcel mass flux is M^P in Pa/s; the entrainment rate, and the mixing and forced detrainment rates are defined in terms of the parcel mass flux as $E = \epsilon M^P$, $N = \mu M^P$, $D = \delta M^P$, where ϵ, μ, δ are the respective coefficients in Pa^{-1}; $q^{(\cdot)}, q_{cl}^{(\cdot)}, q_{cf}^{(\cdot)}$ are the parcel specific humidity, cloud liquid condensate and cloud ice condensate amount in kg/(kg of air); Q denotes the conversion of water vapor into liquid water or ice; P denotes the precipitation fluxes of liquid and ice condensates. Note that the mean quantities over a grid-box are calculated by also accounting for processes occurring within the cloud environment.

Appendix D: Microphysical Transfer Equations (in Qualitative Form)

The equations governing the microphysical transfer of moisture from one species to another, developed by Wilson and Ballard (1999) and based on Rutledge and Hobbs (1983), can be written in qualitative form as:

$$\frac{\mathrm{D}q}{\mathrm{D}t} = (\text{ sublimation of ice aggregates } + \text{ evaporation }) - (\text{ deposition onto aggregates } + \text{ heterogeneous nucleation}), \tag{D1}$$

$$\frac{\mathrm{D}q_{cl}}{\mathrm{D}t} = -(\text{ droplet settling } + \text{ rain autoconversion } + \text{ riming } + \text{ rain accretion } + \text{ heterogeneous nucleation } + \text{ homogeneous nucleation }), \tag{D2}$$

$$\frac{\mathrm{D}q_R}{\mathrm{D}t} = (\text{ fall into layer } - \text{ fall out of layer }) + (\text{ rain autoconversion } + \text{ rain accretion } + \text{ melting }) - (\text{ evaporation } + \text{ capture of raindrops } + \text{ homogeneous nucleation }), \tag{D3}$$

$$\frac{\mathrm{D}q_{cf}}{\mathrm{D}t} = (\text{ fall into layer } - \text{ fall out of layer }) + (\text{ deposition } + \text{ capture of raindrops } + \text{ riming } + \text{ heterogeneous nucleation } + \text{ homogeneous nucleation }) - (\text{ sublimation } + \text{ melting of ice }), \tag{D4}$$

where q, q_{cl}, q_R, q_{cf} are the specific humidity, cloud liquid condensate, rain amount and cloud ice condensate amount in kg/(kg of air) respectively. Note that graupels and ice crystals are not considered. Since generic ice particle size distribution is considered, ice aggregates are the only ice species.

Acknowledgments
SRMN is thankful to Ruth Geen and Mike Byrne for useful discussions. SRMN, FHL, and GKV were supported by NERC CIRCULATES NE/T006285/1. MJW was supported by the Met Office Hadley Centre Climate Programme funded by DSIT. CH was funded by NERC grant NE/T006315/1. DES was supported by a UKRI Future Leaders Fellowship MR/T040866/1. We acknowledge the use of Monsoon2 system, a collaborative facility supplied under the Joint Weather and Climate Research Programme, a strategic partnership between the Met Office and the Natural Environment Research Council, UK. We would like to extend our sincere thanks to the anonymous reviewers for their thoughtful comments which have significantly contributed to the improvement of this manuscript.

Data Availability Statement

Simulation data for the figures are archived at https://doi.org/10.5281/zenodo.8273593 (Natchiar, 2023). We acknowledge the use of the following python libraries: Iris (Met Office, 2010–2013), pandas (The pandas development team, 2020; Wes McKinney, 2010), seaborn (Waskom, 2021), Matplotlib (Hunter, 2007), and aeolus (Sergeev & Zamyatina, 2023).

References

Abel, S. J., Boutle, I. A., Waite, K., Fox, S., Brown, P. R., Cotton, R., et al. (2017). The role of precipitation in controlling the transition from stratocumulus to cumulus clouds in a Northern Hemisphere cold-air outbreak. *Journal of the Atmospheric Sciences*, *74*(7), 2293–2314. https://doi.org/10.1175/jas-d-16-0362.1

Beydoun, H., Caldwell, P. M., Hannah, W. M., & Donahue, A. S. (2021). Dissecting anvil cloud response to sea surface warming. *Geophysical Research Letters*, *48*(15), e2021GL094049. https://doi.org/10.1029/2021gl094049

Bony, S., Stevens, B., Coppin, D., Becker, T., Reed, K. A., Voigt, A., & Medeiros, B. (2016). Thermodynamic control of anvil cloud amount. *Proceedings of the National Academy of Sciences*, *113*(32), 8927–8932. https://doi.org/10.1073/pnas.1601472113

Bordoni, S., & Schneider, T. (2008). Monsoons as eddy-mediated regime transitions of the tropical overturning circulation. *Nature Geoscience*, *1*(8), 515–519. https://doi.org/10.1038/ngeo248

Boutle, I. A., Mayne, N. J., Drummond, B., Manners, J., Goyal, J., Lambert, F. H., et al. (2017). Exploring the climate of Proxima B with the Met Office Unified Model. *Astronomy & Astrophysics*, *601*, A120. https://doi.org/10.1051/0004-6361/201630020

Chaudhuri, A., & Hu, W. (2019). A fast algorithm for computing distance correlation. *Computational Statistics & Data Analysis*, *135*, 15–24. https://doi.org/10.1016/j.csda.2019.01.016

Chen, Y.-W., Seiki, T., Kodama, C., Satoh, M., Noda, A. T., & Yamada, Y. (2016). High cloud responses to global warming simulated by two different cloud microphysics schemes implemented in the Nonhydrostatic Icosahedral Atmospheric Model (NICAM). *Journal of Climate*, *29*(16), 5949–5964. https://doi.org/10.1175/jcli-d-15-0668.1

Derbyshire, S., Maidens, A., Milton, S., Stratton, R., & Willett, M. (2011). Adaptive detrainment in a convective parametrization. *Quarterly Journal of the Royal Meteorological Society*, *137*(660), 1856–1871. https://doi.org/10.1002/qj.875

Field, P. R., Heymsfield, A. J., & Bansemer, A. (2007). Snow size distribution parameterization for midlatitude and tropical ice clouds. *Journal of the Atmospheric Sciences*, *64*(12), 4346–4365. https://doi.org/10.1175/2007jas2344.1

Field, P. R., Hill, A., Shipway, B., Furtado, K., Wilkinson, J., Miltenberger, A., et al. (2023). Implementation of a double moment cloud microphysics scheme in the UK Met Office regional numerical weather prediction model. *Quarterly Journal of the Royal Meteorological Society*, *149*(752), 703–739. https://doi.org/10.1002/qj.4414

Gasparini, B., Blossey, P. N., Hartmann, D. L., Lin, G., & Fan, J. (2019). What drives the life cycle of tropical anvil clouds? *Journal of Advances in Modeling Earth Systems*, *11*(8), 2586–2605. https://doi.org/10.1029/2019ms001736

Gasparini, B., Rasch, P. J., Hartmann, D. L., Wall, C. J., & Duetsch, M. (2021). A Lagrangian perspective on tropical anvil cloud lifecycle in present and future climate. *Journal of Geophysical Research: Atmospheres*, *126*(4), e2020JD033487. https://doi.org/10.1029/2020jd033487

Gasparini, B., Sokol, A. B., Wall, C. J., Hartmann, D. L., & Blossey, P. N. (2022). Diurnal differences in tropical maritime anvil cloud evolution. *Journal of Climate*, *35*(5), 1655–1677. https://doi.org/10.1175/jcli-d-21-0211.1

Gregory, D., & Rowntree, P. (1990). A mass flux convection scheme with representation of cloud ensemble characteristics and stability-dependent closure. *Monthly Weather Review*, *118*(7), 1483–1506. https://doi.org/10.1175/1520-0493(1990)118<1483:amfcsw>2.0.co;2

Harrison, E. F., Minnis, P., Barkstrom, B., Ramanathan, V., Cess, R., & Gibson, G. (1990). Seasonal variation of cloud radiative forcing derived from the Earth Radiation Budget Experiment. *Journal of Geophysical Research*, *95*(D11), 18687–18703. https://doi.org/10.1029/jd095id11p18687

Hartmann, D. L. (2016). Tropical anvil clouds and climate sensitivity. *Proceedings of the National Academy of Sciences*, *113*(32), 8897–8899. https://doi.org/10.1073/pnas.1610455113

Hartmann, D. L., & Berry, S. E. (2017). The balanced radiative effect of tropical anvil clouds. *Journal of Geophysical Research: Atmospheres*, *122*(9), 5003–5020. https://doi.org/10.1002/2017jd026460

Hartmann, D. L., Gasparini, B., Berry, S. E., & Blossey, P. N. (2018). The life cycle and net radiative effect of tropical anvil clouds. *Journal of Advances in Modeling Earth Systems*, *10*(12), 3012–3029. https://doi.org/10.1029/2018ms001484

Hartmann, D. L., & Larson, K. (2002). An important constraint on tropical cloud-climate feedback. *Geophysical Research Letters*, *29*(20), 12-1–12-4. https://doi.org/10.1029/2002gl015835

Hunter, J. D. (2007). Matplotlib: A 2D graphics environment [Software]. *Computing in Science & Engineering*, *9*(3), 90–95. https://doi.org/10.1109/MCSE.2007.55

Igel, A. L., Igel, M. R., & van den Heever, S. C. (2015). Make it a double? Sobering results from simulations using single-moment microphysics schemes. *Journal of the Atmospheric Sciences*, *72*(2), 910–925. https://doi.org/10.1175/jas-d-14-0107.1

Jeevanjee, N. (2022). Three rules for the decrease of tropical convection with global warming. *Journal of Advances in Modeling Earth Systems*, *14*(11), e2022MS003285. https://doi.org/10.1029/2022ms003285

Jenney, A. M., Randall, D. A., & Branson, M. (2020). Understanding the response of tropical ascent to warming using an energy balance framework. *Journal of Advances in Modeling Earth Systems*, *12*(6), e2020MS002056. https://doi.org/10.1029/2020ms002056

Kim, D., Kim, H., Kang, S. M., Stuecker, M. F., & Merlis, T. M. (2022). Weak Hadley cell intensity changes due to compensating effects of tropical and extratropical radiative forcing. *npj Climate and Atmospheric Science*, *5*(1), 61. https://doi.org/10.1038/s41612-022-00287-x

Knutson, T. R., & Manabe, S. (1995). Time-mean response over the tropical Pacific to increased CO_2 in a coupled ocean-atmosphere model. *Journal of Climate*, *8*(9), 2181–2199. https://doi.org/10.1175/1520-0442(1995)008<2181:tmrott>2.0.co;2

Kuang, Z., & Hartmann, D. L. (2007). Testing the fixed anvil temperature hypothesis in a cloud-resolving model. *Journal of Climate*, *20*(10), 2051–2057. https://doi.org/10.1175/jcli4124.1

Met Office. (2010–2013). Iris: A python package for analysing and visualising meteorological and oceanographic data sets (v1.2 ed.) [Computer software manual]. *Exeter, Devon*. Retrieved from http://scitools.org.uk/

Morrison, H., van Lier-Walqui, M., Fridlind, A. M., Grabowski, W. W., Harrington, J. Y., Hoose, C., et al. (2020). Confronting the challenge of modeling cloud and precipitation microphysics. *Journal of Advances in Modeling Earth Systems*, *12*(8), e2019MS001689. https://doi.org/10.1029/2019ms001689

Natchiar, S. R. M. (2023). Reduction in the tropical high cloud fraction in response to an indirect weakening of the Hadley cell [Dataset]. *Zenodo*. https://doi.org/10.5281/zenodo.8273593

Ohno, T., Noda, A. T., Seiki, T., & Satoh, M. (2021). Importance of pressure changes in high cloud area feedback due to global warming. *Geophysical Research Letters*, *48*(18), e2021GL093646. https://doi.org/10.1029/2021gl093646

Ohno, T., & Satoh, M. (2018). Roles of cloud microphysics on cloud responses to sea surface temperatures in radiative-convective equilibrium experiments using a high-resolution global nonhydrostatic model. *Journal of Advances in Modeling Earth Systems*, *10*(8), 1970–1989. https://doi.org/10.1029/2018ms001386

Ohno, T., Satoh, M., & Noda, A. (2019). Fine vertical resolution radiative-convective equilibrium experiments: Roles of turbulent mixing on the high-cloud response to sea surface temperatures. *Journal of Advances in Modeling Earth Systems*, *11*(6), 1637–1654. https://doi.org/10.1029/2019ms001704

Ramanathan, V., Cess, R., Harrison, E., Minnis, P., Barkstrom, B., Ahmad, E., & Hartmann, D. (1989). Cloud-radiative forcing and climate: Results from the Earth Radiation Budget Experiment. *Science*, *243*(4887), 57–63. https://doi.org/10.1126/science.243.4887.57

Rutledge, S. A., & Hobbs, P. (1983). The mesoscale and microscale structure and organization of clouds and precipitation in midlatitude cyclones. VIII: A model for the "seeder-feeder" process in warm-frontal rainbands. *Journal of the Atmospheric Sciences*, *40*(5), 1185–1206. https://doi.org/10.1175/1520-0469(1983)040<1185:tmamsa>2.0.co;2

Saint-Lu, M., Bony, S., & Dufresne, J.-L. (2020). Observational evidence for a stability Iris effect in the tropics. *Geophysical Research Letters*, *47*(14), e2020GL089059. https://doi.org/10.1029/2020gl089059

Schiro, K. A., Su, H., Wang, Y., Langenbrunner, B., Jiang, J. H., & Neelin, J. D. (2019). Relationships between tropical ascent and high cloud fraction changes with warming revealed by perturbation physics experiments in CAM5. *Geophysical Research Letters*, *46*(16), 10112–10121. https://doi.org/10.1029/2019gl083026

Seeley, J. T., Jeevanjee, N., Langhans, W., & Romps, D. M. (2019). Formation of tropical anvil clouds by slow evaporation. *Geophysical Research Letters*, *46*(1), 492–501. https://doi.org/10.1029/2018gl080747

Sergeev, D. E., & Zamyatina, M. (2023). aeolus [Software]. *Zenodo*. https://doi.org/10.5281/zenodo.7829974

Sherwood, S., Webb, M. J., Annan, J. D., Armour, K. C., Forster, P. M., Hargreaves, J. C., et al. (2020). An assessment of earth's climate sensitivity using multiple lines of evidence. *Reviews of Geophysics*, *58*(4), e2019RG000678. https://doi.org/10.1029/2019rg000678

Singh, M. S., & Kuang, Z. (2016). Exploring the role of eddy momentum fluxes in determining the characteristics of the equinoctial Hadley circulation: Fixed-SST simulations. *Journal of the Atmospheric Sciences*, *73*(6), 2427–2444. https://doi.org/10.1175/jas-d-15-0212.1

Singh, M. S., Kuang, Z., & Tian, Y. (2017). Eddy influences on the strength of the Hadley circulation: Dynamic and thermodynamic perspectives. *Journal of the Atmospheric Sciences*, *74*(2), 467–486. https://doi.org/10.1175/jas-d-16-0238.1

Singh, M. S., & O'Gorman, P. A. (2015). Increases in moist-convective updraught velocities with warming in radiative-convective equilibrium. *Quarterly Journal of the Royal Meteorological Society*, *141*(692), 2828–2838. https://doi.org/10.1002/qj.2567

Smith, R. (1990). A scheme for predicting layer clouds and their water content in a general circulation model. *Quarterly Journal of the Royal Meteorological Society*, *116*(492), 435–460. https://doi.org/10.1002/qj.49711649210

Sokol, A. B., & Hartmann, D. L. (2022). Radiative cooling, latent heating, and cloud ice in the tropical upper troposphere. *Journal of Climate*, *35*(5), 1643–1654. https://doi.org/10.1175/jcli-d-21-0444.1

Stauffer, C. L., & Wing, A. A. (2022). Properties, changes, and controls of deep-convecting clouds in radiative-convective equilibrium. *Journal of Advances in Modeling Earth Systems*, *14*(6), e2021MS002917. https://doi.org/10.1029/2021ms002917

Székely, G. J., Rizzo, M. L., & Bakirov, N. K. (2007). Measuring and testing dependence by correlation of distances. *Annals of Statistics*, *35*(6), 2769–2794. https://doi.org/10.1214/009053607000000505

The pandas development team. (2020). pandas-dev/pandas: Pandas [Software]. *Zenodo*. https://doi.org/10.5281/zenodo.3509134

Tsushima, Y., Iga, S.-I., Tomita, H., Satoh, M., Noda, A. T., & Webb, M. J. (2014). High cloud increase in a perturbed SST experiment with a global nonhydrostatic model including explicit convective processes. *Journal of Advances in Modeling Earth Systems*, *6*(3), 571–585. https://doi.org/10.1002/2013ms000301

Walters, D., Baran, A. J., Boutle, I., Brooks, M., Earnshaw, P., Edwards, J., et al. (2019). The Met Office Unified Model global atmosphere 7.0/7.1 and JULES global land 7.0 configurations. *Geoscientific Model Development*, *12*(5), 1909–1963. https://doi.org/10.5194/gmd-12-1909-2019

Waskom, M. L. (2021). Seaborn: Statistical data visualization [Software]. *Journal of Open Source Software*, *6*(60), 3021. https://doi.org/10.21105/joss.03021

Wes McKinney. (2010). Data structures for statistical computing in Python [Software]. In S. van der Walt, & J. Millman (Eds.), *Proceedings of the 9th Python in Science Conference* (pp. 56–61). https://doi.org/10.25080/Majora-92bf1922-00a

Wilson, D. R., & Ballard, S. P. (1999). A microphysically based precipitation scheme for the UK meteorological office Unified Model. *Quarterly Journal of the Royal Meteorological Society*, *125*(557), 1607–1636. https://doi.org/10.1256/smsqj.55706

Wilson, D. R., Bushell, A. C., Kerr-Munslow, A. M., Price, J. D., & Morcrette, C. J. (2008). PC2: A prognostic cloud fraction and condensation scheme. I: Scheme description. *Quarterly Journal of the Royal Meteorological Society*, *134*(637), 2093–2107. https://doi.org/10.1002/qj.333

Wing, A. A., Stauffer, C. L., Becker, T., Reed, K. A., Ahn, M.-S., Arnold, N. P., et al. (2020). Clouds and convective self-aggregation in a multimodel ensemble of radiative-convective equilibrium simulations. *Journal of Advances in Modeling Earth Systems*, *12*(9), e2020MS002138. https://doi.org/10.1029/2020ms002138

Yanai, M., Esbensen, S., & Chu, J. (1973). Determination of bulk properties of tropical cloud clusters from large-scale heat and moisture budgets. *Journal of the Atmospheric Sciences*, *30*(4), 611–627. https://doi.org/10.1175/1520-0469(1973)030<0611:dobpot>2.0.co;2

Zelinka, M. D., & Hartmann, D. L. (2010). Why is longwave cloud feedback positive? *Journal of Geophysical Research*, *115*(D16), D16117. https://doi.org/10.1029/2010jd013817

Zelinka, M. D., & Hartmann, D. L. (2011). The observed sensitivity of high clouds to mean surface temperature anomalies in the tropics. *Journal of Geophysical Research*, *116*(D23), D23103. https://doi.org/10.1029/2011jd016459